RSC Advances

ROYAL SOCIETY OF CHEMISTRY

www.rsc.org/advances

RSC Advances

ARTICLE

Effect of valence states of Ni and Mn on the structural and electrochemical properties of $Li_{1.2}Ni_xMn_{0.8-x}O_2$ cathode materials for lithium-ion batteries

Received 00th January 20xx,
Accepted 00th January 20xx

DOI: 10.1039/x0xx00000x

www.rsc.org/

Shaokun Chong, Yongning Liu,* Wuwei Yan and Yuanzhen Chen

Severe capacity fading and voltage decay of Li-rich layered oxides for lithium-ion batteries remain to be the major bottlenecks to commercialization. Herein, we studied the effect of valence states of Ni and Mn on the structure and electrochemical performances of $Li_{1.2}Ni_xMn_{0.8-x}O_2$. The oxidation states of transition-metal (TM) were evaluated by X-ray photoelectron spectra (XPS) and validated by cyclic voltammetry (CV). With increasing Mn^{3+} content, Li_2MnO_3 component increases due to less Li loss. The phenomenon of capacity increase upon cycling has been observed owing to the gradual activation of Li_2MnO_3 caused by the existence of Mn^{3+}. It is worth mentioning that $Li_{1.2}Ni_{0.1}Mn_{0.7}O_2$ reaches the highest discharge capacity value of 231.5 mAh·g^{-1} from the initial value of 76 mAh·g^{-1} after 75 cycles and still keeps 100% of the capacity at 0.1C after 100 cycles. As the increase of Ni^{3+}, Li/Ni mixing decreases because of its smaller size than Ni^{2+}, the content of Li_2MnO_3 decreases as a result of the decrease of Li and Mn in the TM layers, and the discharge voltage increases on account of the higher reduction potential of Ni^{4+}/Ni^{3+} compared with Ni^{4+}/Ni^{2+} and Mn^{4+}/Mn^{3+}. Furthermore, $Li_{1.2}Ni_{0.4}Mn_{0.4}O_2$ delivers the first capacity value of 192.5 mAh·g^{-1} and operating voltage of 3.89 V at 0.1C, and capacity retention with 92.13% and the voltage drop of 0.25 V after 100 cycles, which indicates that the stability of capacity and voltage is improved by a large margin with increasing the Ni^{3+}.

1. Introduction

Rechargeable lithium-ion secondary batteries are considered as the most valuable energy storage devices for mobile phones, laptops and electric vehicles due to high energy density, safety and long cycle life [1, 2]. Nowadays, the most conventional cathode materials are layered oxides $LiMO_2$ (M=Ni, Co and Mn) with excellent cyclability, olivine $LiFePO_4$ with low cost and long cycle life, and spinel oxides $LiMn_2O_4$ and $LiNi_{0.5}Mn_{1.5}O_4$ with high voltage, while all of them suffer from low discharge capacity and fail to meet the requirements of high energy density for practical applications [3, 4].

Recently, a layered cathode material with a chemical formula of xLi_2MnO_3-(1-x)$LiMO_2$ (M=Ni, Co and Mn) attracts wide attention owing to its higher discharge capacity (more than 250 mAh·g^{-1}) and much higher operating voltage (about 3.5 V) [5, 6]. However, there are many remaining problems have to be solved, such as low initial coulombic efficiency, poor rate performance, serious capacity fading and voltage decay. The low initial coulombic efficiency is associated with the release of irreversible oxygen along with the activation of Li_2MnO_3 during the first charge process, resulting in the formation of oxide ion vacancies [7]. The poor rate performance is related to the weak intrinsic electronic conductivity resulted from insulated Li_2MnO_3 component and the thick solid-electrolyte interphase (SEI) layer [8]. The serious capacity fading and voltage decay should be attributed to the fast layer-spinel phase transformation, which leads to a fast reduction in energy density [3, 9].

$Li_{1.2}Ni_{0.2}Mn_{0.6}O_2$ cathode material has become a hotspot research because of its high initial discharge capacity recently [10-13], while the problems of serious capacity fading and voltage decay caused by layered-spinel structural transformation upon cycling have not been solved radically. Thus, it is necessary to study the other cathode materials with a chemical formula of $Li_{1.2}Ni_xMn_{0.8-x}O_2$ and understand what factors affect the discharge capacity and voltage decay and further what measures should be taken to optimize the structure and ameliorate properties. It is reported that the existence of Mn^{3+} facilitates the activation of Li_2MnO_3 phase, which gives rise to a higher discharge specific capacity after the complete activation of Li_2MnO_3. Unfortunately, the gradual activation of Li_2MnO_3 induces faster layered-spinel transformation, leading to rapid capacity fading [14, 15]. In addition, Knight *et al.* have investigated the effect of Ni oxidation state on the structural and electrochemical characteristics, proposing Ni^{3+} can improve the cyclability and mitigate voltage decay [16], while the valence of Ni and the actual content of Li haven't been measured by any characterization methods.

Herein, we report a layered oxides with a chemical formula of $Li_{1.2}Ni_xMn_{0.8-x}O_2$ (x=0, 0.1, 0.2, 0.3 and 0.4) prepared by a simple combustion method and a detailed study of the oxidation states of TM on the structure and electrochemical performances for the Li-

State Key Laboratory for Mechanical Behavior of Materials, School of Material Science and Engineering, Xi'an Jiaotong University, Xi'an 710049, PR China. Email:ynliu@mail.xjtu.edu.cn; Fax: +86 29 8266 3453; Tel: +86 29 8266 4602

rich cathode materials by changing the relative proportion of Ni and Mn. It should be noted that, the phenomenon of capacity increase upon cycling is observed by reason of the existence of Mn^{3+}, which leads to a much higher capacity and more excellent cyclability. In addition, the stability of capacity and voltage is improved by a large margin with increasing the Ni^{3+}. The findings herein may shed light not only on the effects understanding of the oxidation states of TM in Li-rich oxides but also on the design and improvement measures of high energy density lithium-ion batteries by controlling the content of Mn^{3+} and Ni^{3+}.

2. Experimental

2.1 Synthesis of $Li_{1.2}Ni_xMn_{0.8-x}O_2$

The $Li_{1.2}Ni_xMn_{0.8-x}O_2$ (x=0, 0.1, 0.2, 0.3 and 0.4) cathode materials were synthesized by a facile combustion method using Li, Ni, Mn acetates and citric acid as starting materials. Stoichiometric amounts of $C_2H_3O_2Li{\cdot}2H_2O$, $C_4H_6NiO_4{\cdot}4H_2O$ and $C_4H_6MnO_4{\cdot}4H_2O$ (Sinopharm Chemical Reagent) were dissolved in ethanol under magnetic stirring to form solution A and $C_6H_8O_7{\cdot}H_2O$ (Sinopharm Chemical Reagent) was dissolved in ethanol to form solution B. A 5% excess of Li was used to offset the loss of Li during sintering under high temperature and the molar ratio of metal and citric acid was 1:1. Then solution A and solution B were instilled separately into 100 ml ethanol base solution under continuous mechanical stirring. The base solution turned into white emulsion gradually as ethanol was evaporated at 80 °C and further dried at 110 °C for 12 h to obtain precursor. Finally the mixture was calcined at 450 °C for 5 h in air to remove the organics and then heated at 900 °C for 5 h in air with heating rates of 3 °C/min.

2.2 Material characterization

X-ray photoelectron spectra (XPS, Axis Ultrabld, Kratos) was used to detect the surface elemental chemical state of $Li_{1.2}Ni_xMn_{0.8-x}O_2$ (x=0, 0.1, 0.2, 0.3 and 0.4) cathode materials. The actual elemental chemical composition of the samples was determined by a Varian 715-ES inductively coupled plasma atomic emission spectroscopy (ICP-AES). The crystal structures of prepared materials were identified by X-ray diffraction (XRD, UltimaIV-185, Rigaku) using Cu Kα radiation at 40 mA and 40 kV in the range of 10-80°.

2.3 Electrochemical characterization

The electrochemical performance of $Li_{1.2}Ni_xMn_{0.8-x}O_2$ (x=0, 0.1, 0.2, 0.3 and 0.4) cathode materials was measured on a battery test system (Neware, China) using a CR2025-type coin-cell. The cathode electrode was fabricated by coating an aluminum foil with a slurry which consisted of 80 wt.% active material, 10 wt.% acetylene black and 10 wt.% polyvinylidene fluoride (PVDF) in N-methyl pyrrolidinone (NMP). Then the aluminum foil was dried at 100 °C for 12 h in a vacuum oven and was punched out a round cathode electrode disk of diameter 12 mm. Coin cells were assembled in an Argon-filled glove box (Super 1220/750, Mikrouna) using fabricated round electrode disk as cathode, lithium foil as anode, celgard 2300 porous polypropylene film as separator and 1 M $LiPF_6$ in EC/DMC/DEC (1:1:1, Vol%) as electrolyte. The galvanostatic charge/discharge was measured with a current density of 20 $mA{\cdot}g^{-1}$ (0.1C) between 2.0 V and 4.8 V (vs. Li/Li+) at room temperature. Cyclic voltammetry (CV) was performed on a CHI750D electrochemical workstation in the potential range of 2.0-4.8 V at a scanning rate of 0.1 $mV{\cdot}s^{-1}$.

3. Results and discussion

3.1 Structure

From chemical point of view, the Mn and Ni ions in $Li_{1.2}Ni_{0.2}Mn_{0.6}O_2$ (x=0.2) are expected to show the +4 and +2 oxidation states, respectively [11]. In order to maintain the chemical formula, the valence states of TM ions in the synthesized $Li_{1.2}Ni_xMn_{0.8-x}O_2$ are $Li_{1.2}Mn^{3+/4+}{}_{0.8}O_2$ (x=0), $Li_{1.2}Ni^{2+}{}_{0.1}Mn^{3+/4+}{}_{0.7}O_2$ (x=0.1), $Li_{1.2}Ni^{2+/3+}{}_{0.3}Mn^{4+}{}_{0.5}O_2$ (x=0.3) and $Li_{1.2}Ni^{3+}{}_{0.4}Mn^{4+}{}_{0.4}O_2$ (x=0.4), respectively.

XPS was used to determine the exact oxidation states of Mn and Ni in the layered composite material, the corresponding spectra are presented in Fig. 1. Mn_{2p} peaks of $Li_{1.2}Mn_{0.8}O_2$ (Fig. 1a), $Li_{1.2}Ni_{0.1}Mn_{0.7}O_2$ (Fig. 1b), $Li_{1.2}Ni_{0.2}Mn_{0.6}O_2$ (Fig. 1d), $Li_{1.2}Ni_{0.3}Mn_{0.5}O_2$ (Fig. 1f) and $Li_{1.2}Ni_{0.4}Mn_{0.4}O_2$ (Fig. 1h) can be fitted by multiple peaks with binding energies (BEs) (reported BEs of Mn^{3+} and Mn^{4+} are: 640.6 eV and 641.4-644.8 eV, respectively) [14], the fitting results and relative percentage of Mn^{3+} and Mn^{4+} shown in Fig. 2. This means that the oxidation states of Mn for $Li_{1.2}Ni_{0.2}Mn_{0.6}O_2$, $Li_{1.2}Ni_{0.3}Mn_{0.5}O_2$ and $Li_{1.2}Ni_{0.4}Mn_{0.4}O_2$ present 4+. However, Mn ions in $Li_{1.2}Ni_{0.1}Mn_{0.7}O_2$ and $Li_{1.2}Mn_{0.8}O_2$ consist of Mn^{3+} (40.3%) and Mn^{4+} (59.7%), Mn^{3+} (49.6%) and Mn^{4+} (50.4%), respectively. The existence of Mn^{3+} can also be proved by the oxidation peak of Mn^{3+}/Mn^{4+} during initial charge process in Fig. 4 (b and c). The Ni spectra are shown in Fig. 1c ($Li_{1.2}Ni_{0.1}Mn_{0.7}O_2$), Fig. 1e ($Li_{1.2}Ni_{0.2}Mn_{0.6}O_2$), Fig. 1g ($Li_{1.2}Ni_{0.3}Mn_{0.5}O_2$) and Fig. 1i ($Li_{1.2}Ni_{0.4}Mn_{0.4}O_2$). $Ni_{2p3/2}$ peak fitting procedure reveals two types of BEs: 853.7-855 eV [17, 18] and 855.3-855.9eV [19]. The lower BEs is in agreement with that of $Li[Li_{1/3-2x/3}Ni_xMn_{2/3-x/3}]O_2$ compounds, which confirms the presence of Ni^{2+}, and the higher BEs is consistent with that of $LiNiO_2$, which proves the presence of Ni^{3+}. The fitting results in Fig. 2 reveal that the valence states of Ni in $Li_{1.2}Ni_{0.1}Mn_{0.7}O_2$ and $Li_{1.2}Ni_{0.2}Mn_{0.6}O_2$ are all +2. However, Ni ions in $Li_{1.2}Ni_{0.3}Mn_{0.5}O_2$ and $Li_{1.2}Ni_{0.4}Mn_{0.4}O_2$ are composed of Ni^{2+} (87.9%) and Ni^{3+} (12.1%), Ni^{2+} (19.9%) and Ni^{3+} (80.1%), respectively. Therefore, the experimentally determined oxidation states of TM ions are basically consistent with the theoretical ones.

ICP-AES analysis results of $Li_{1.2}Ni_xMn_{0.8-x}O_2$ (x=0, 0.1, 0.2, 0.3 and 0.4) are shown in Table 1. The accurate elemental ratios of Ni/Mn are in excellent agreement with nominal values and the relative lithium content of $Li_{1.2}Ni_{0.2}Mn_{0.6}O_2$ are well close to target stoichiometries. However, the relative lithium contents of all samples decreased with increasing x value. Owing to the appearance of Ni^{3+} and the difficulty in maintaining Ni^{3+} content, more than 5% extra Li was used to compensate the Li loss during high temperature heating for $Li_{1.2}Ni_{0.3}Mn_{0.5}O_2$ and $Li_{1.2}Ni_{0.4}Mn_{0.4}O_2$ [16]. Furthermore, $Li_{1.2}Mn_{0.8}O_2$ required little excess of Li and $Li_{1.2}Ni_{0.1}Mn_{0.7}O_2$ required less than 5% of Li to counteract the Li loss for producing the desired composition thanks to the fact that more Mn^{4+} was replaced by Mn^{3+} and there's no need to maintain the Mn^{4+} to increase in the degree of lithium volatilization.

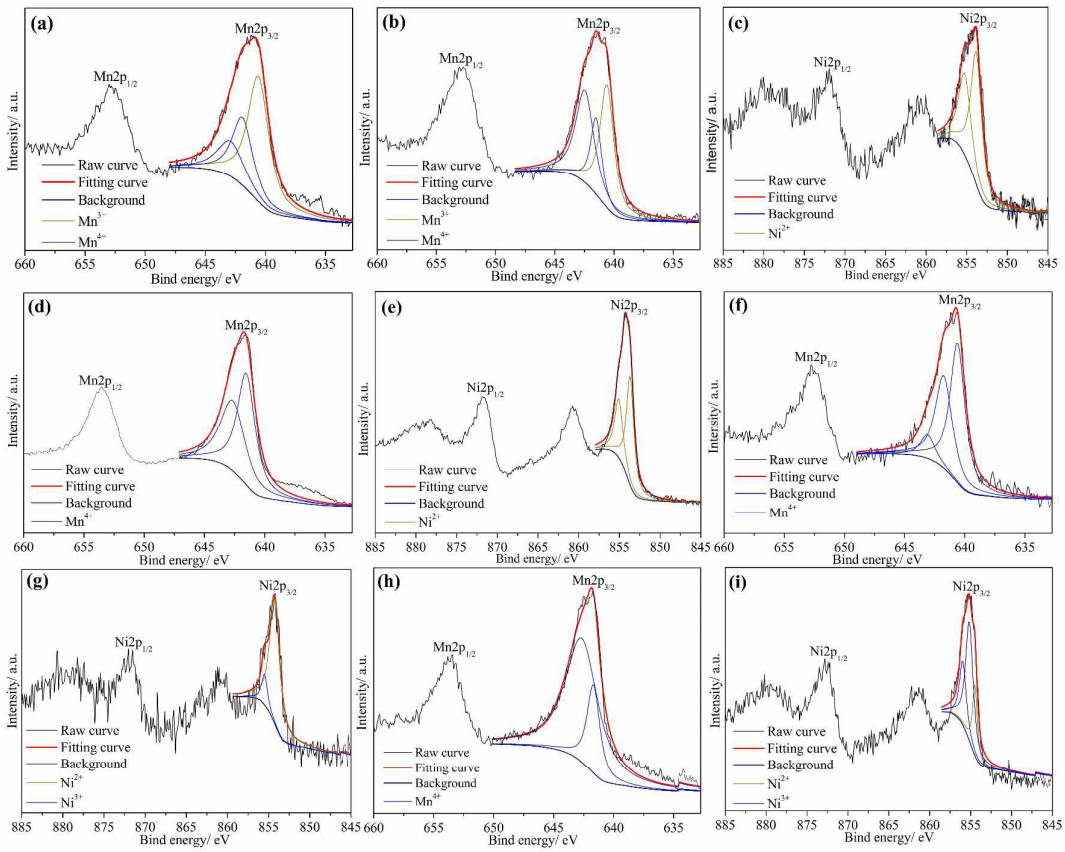

Fig. 1 Fitting results of XPS spectra of (a) Mn_{2p} for $Li_{1.2}Mn_{0.8}O_2$. (b and c) Mn_{2p} and Ni_{2p} for $Li_{1.2}Ni_{0.1}Mn_{0.7}O_2$. (d and e) Mn_{2p} and Ni_{2p} for $Li_{1.2}Ni_{0.2}Mn_{0.6}O_2$. (f and g) Mn_{2p} and Ni_{2p} for $Li_{1.2}Ni_{0.3}Mn_{0.5}O_2$. (h and i) Mn_{2p} and Ni_{2p} for $Li_{1.2}Ni_{0.4}Mn_{0.4}O_2$.

Table1 ICP-AES analysis results and lattice parameters and the ratios of *I(003)/I(104)* calculated from the XRD data

x	Sample	ICP results	a/Å	c/Å	*c/a*	*I(003)/I(104)*
0	$Li_{1.2}Mn_{0.8}O_2$	$Li_{1.249}Mn_{0.8}O_2$	2.8647	14.2159	4.962	1.781
0.1	$Li_{1.2}Ni_{0.1}Mn_{0.7}O_2$	$Li_{1.226}Ni_{0.1}Mn_{0.702}O_2$	2.8737	14.2984	4.976	0.671
0.2	$Li_{1.2}Ni_{0.2}Mn_{0.6}O_2$	$Li_{1.204}Ni_{0.2}Mn_{0.599}O_2$	2.8676	14.2765	4.979	0.948
0.3	$Li_{1.2}Ni_{0.3}Mn_{0.5}O_2$	$Li_{1.114}Ni_{0.3}Mn_{0.501}O_2$	2.8779	14.2874	4.965	1.287
0.4	$Li_{1.2}Ni_{0.4}Mn_{0.4}O_2$	$Li_{0.991}Ni_{0.4}Mn_{0.399}O_2$	2.8799	14.2990	4.965	1.433

Fig. 3(a) shows the XRD patterns of $Li_{1.2}Ni_xMn_{0.8-x}O_2$ (x=0, 0.1, 0.2, 0.3 and 0.4). The main diffraction peaks can be indexed as a hexagonal α-$NaFeO_2$ layered structure with the $R\bar{3}m$ space group. The clear splitting of (006)/(102) and (018)/(110) doublets indicate the formation of a highly ordered layered structure for all samples [20, 21]. The lattice parameters calculated from the XRD data are listed in Table 1. The c/a ratios of all samples are more than 4.9, which further provides the evidence for an explicit crystalline layer structure [22, 23]. Moreover, the ratio of $I_{(003)}/I_{(104)}$ can be used to evaluate the degree of the cation mixing between Li^+ and Ni^{2+} in the Li-layers, and the value of $I_{(003)}/I_{(104)}$ > 1.2 is an indication of low degree of cation dislocation [24, 25]. It is indicated that there is no cation mixing in $Li_{1.2}Mn_{0.8}O_2$ because the content of Ni is 0. However, the values of $I_{(003)}/I_{(104)}$ for $Li_{1.2}Ni_{0.1}Mn_{0.7}O_2$ and $Li_{1.2}Ni_{0.2}Mn_{0.6}O_2$ are respectively 0.671 and 0.948, which are both lower than 1.2, indicating more cation dislocation between Li^+ and Ni^{2+}. For $Li_{1.2}Ni_{0.3}Mn_{0.5}O_2$ and $Li_{1.2}Ni_{0.4}Mn_{0.4}O_2$, the values of $I_{(003)}/I_{(104)}$ are higher than 1.2, indicating lower level of cation disordering. As can be seen from above, the ratio of (003)/(104) peak increases as the Ni^{3+} increases because Ni^{3+} ions (0.56Å) are much smaller than Ni^{2+} ions (0.69Å) and Li^+ ions (0.76Å), which leads to lower Li/Ni site mixing [16].

The weak peaks between 20-22.5° are attributed to short-range superlattice ordering of Li and Mn in the TM layers of the layered Li_2MnO_3 region, which can be indexed to the monoclinic unit cell with the C2/m space group [26-28]. In the magnified XRD patterns (20.0-22.5°) shown in Fig. 3(b), the intensity of these weak peaks appear much more intense with increasing the content of Mn, resulting from a few Li loss during high temperature heating process and more Li content in the TM layers. However, a cubic spinel structure with a space group of Fd3m can be detected in the XRD pattern (Fig. 1a) for $Li_{1.2}Mn_{0.8}O_2$.

3.2 Electrochemical performance

3.2.1 Initial charge and discharge behavior

To evaluate the effect of valence states of Ni and Mn on the initial electrochemical performance of $Li_{1.2}Ni_xMn_{0.8-x}O_2$ (x=0, 0.1, 0.2, 0.3 and 0.4), the initial charge-discharge curves and corresponding cyclic voltammetry profiles of all the five samples measured at a constant current density of 20 $mA{\cdot}g^{-1}$ (0.1C) between 2.0 V and 4.8 V are shown in Fig. 4. As normal $Li_{1.2}Ni_{0.2}Mn_{0.6}O_2$ layered oxides, a sloping and a plateau are observed during the initial charge process in Fig. 4(a). The sloping curve below 4.5 V is ascribed to the lithium extraction from $LiMO_2$ (M=Ni, Mn) component accompanied by oxidation of $Ni^{2+}/Ni^{3+}/Ni^{4+}$. And the long plateau above 4.5 V is attributed to the lithium extraction from Li_2MO_3 component with the reaction of O^{2-}/O_2 redox couple [29, 30], which represents the activation of Li_2MO_3. It can be seen obviously that $Li_{1.2}Ni_{0.2}Mn_{0.6}O_2$ delivers the highest initial charge and discharge capacity in Fig. 4(a). The corresponding CV curve shows the oxidation peak of $Ni^{2+}/Ni^{3+}/Ni^{4+}$ at about 3.85 V as well as the irreversible activation process of Li_2MO_3 region at about 4.7 V during initial charge process, and a broad Ni reduction peak at about 3.7 V as well as a very weak reduction peak corresponding to Mn^{4+}/Mn^{3+} couple at

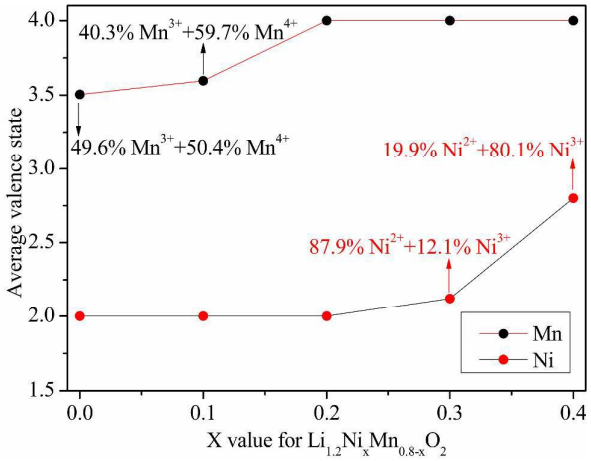

Fig. 2 Average valence states of transition metal in $Li_{1.2}Ni_xMn_{0.8-x}O_2$.

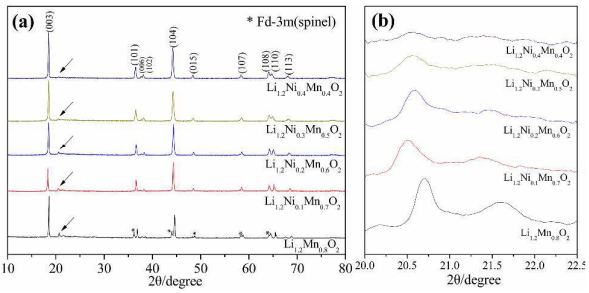

Fig. 3 (a) XRD patterns of $Li_{1.2}Ni_xMn_{0.8-x}O_2$ (x=0, 0.1, 0.2, 0.3 and 0.4), respectively. (b) Expanded regions of XRD patterns of all samples within a 2θ range of 20.0-22.5°, respectively.

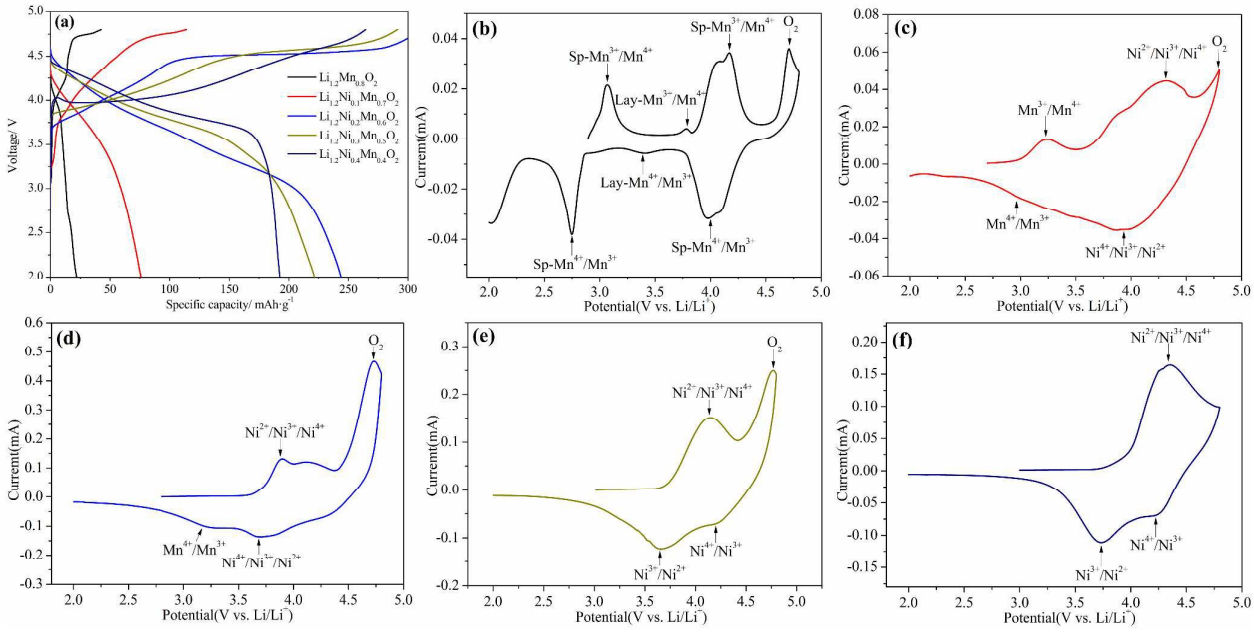

Fig. 4 (a) Initial charge and discharge curves of all five samples at 0.1C between 2.0 and 4.8 V. (b, c, d, e and f) Corresponding cyclic voltammetry profiles.

approximately 3.2 V during initial discharge process in Fig. 4(d).

However, the capacity of sloping below 4.5 V and plateau above 4.5 V decrease as the content of Mn^{3+} increases, which leads to a much lower initial charge and discharge capacity for $Li_{1.2}Mn_{0.8}O_2$ and $Li_{1.2}Ni_{0.1}Mn_{0.7}O_2$. For $Li_{1.2}Ni_{0.1}Mn_{0.7}O_2$, the much lower sloping capacity is most likely attributable to the serious Li/Ni site mixing. Also, the appearance of Mn^{3+} suppresses the complete activation of Li_2MO_3 [14], resulting in shorter plateau above 4.5 V. The most of peaks for the CV curve of $Li_{1.2}Ni_{0.1}Mn_{0.7}O_2$ in Fig. 4(c) are similar to $Li_{1.2}Ni_{0.2}Mn_{0.6}O_2$, while an oxidation peak at approximately 3.25 V of Mn^{3+}/Mn^{4+} is observed, which provides an evidence of Mn^{3+} ion formation in consistent with the result of XPS. For $Li_{1.2}Mn_{0.8}O_2$, the much lower capacity can be attributed to two factors. On the one hand, the presence of $Li_{1+x}Mn_{2-x}O_4$ with the spinel structure leads to the diminished sloping capacity [31]. On the other hand, Mn^{3+} and spinel structure suppress irreversible extraction of Li^+ and O^{2-} from Li_2MnO_3 component during the first charge process [14, 31]. Furthermore, the CV of $Li_{1.2}Mn_{0.8}O_2$ is particularly informative. Two intense oxidation peaks of Mn^{3+}/Mn^{4+} at 3.1 V and 4.25 V are observed clearly, characteristic of a Li-Mn oxide spinel phase in the system $Li_{1+x}Mn_{2-x}O_4$ [30, 32], except for the normal oxidation peak of Mn^{3+}/Mn^{4+} in layer $LiMnO_2$ at about 3.8 V and a much weaker irreversible activation of Li_2MO_3 at about 4.7 V during initial charge process in Fig. 4(b), which is consistent with the result of XPS and XRD.

Obviously, the capacity of sloping below 4.5 V becomes higher with the increase of Ni^{3+} on account of much lower level of Li/Ni cation mixing. On the contrary, the capacity of plateau above 4.5 V decreases with increasing the content Ni^{3+}, resulting in a much lower plateau capacity for $Li_{1.2}Ni_{0.3}Mn_{0.5}O_2$ and disappearence of plateau for $Li_{1.2}Ni_{0.4}Mn_{0.4}O_2$. This is most likely due to the reduction in the Li^+ and Mn^{4+}, resulting in decreasing the Li_2MnO_3 component [16]. The CV profiles show the oxidation peaks of $Ni^{2+}/Ni^{3+}/Ni^{4+}$ at about 4.2 V and 4.3 V for $Li_{1.2}Ni_{0.3}Mn_{0.5}O_2$ (Fig. 4e) and $Li_{1.2}Ni_{0.4}Mn_{0.4}O_2$ (Fig. 4f), respectively. However, the corresponding reduction peak splits into two separate peaks because the voltage difference between Ni^{3+}/Ni^{2+} and Ni^{4+}/Ni^{3+} redox couples [33]. Moreover, the peak of Li_2MnO_3 activation can't be observed for $Li_{1.2}Ni_{0.4}Mn_{0.4}O_2$ during the initial charge process, in accordance with the disappearance of plateau and the results of XRD. In addition, it is clear that the discharge median voltage in the initial cycle increases with increasing the content of Ni^{3+}, because Ni^{3+} shows the much higher redox potential compared with Ni^{2+} and Mn^{3+}.

3.2.2 Cyclic performance

The cyclic performances of $Li_{1.2}Ni_xMn_{0.8-x}O_2$ (x=0, 0.1, 0.2, 0.3 and 0.4) at 20 $mA{\cdot}g^{-1}$ (0.1C) in the voltage range of 2.0-4.8 V for the first 100 cycles are shown in Fig. 5(a). $Li_{1.2}Ni_{0.2}Mn_{0.6}O_2$ exhibits the highest initial discharge capacity of 244 $mAh{\cdot}g^{-1}$, while it shows only capacity retention of 62.97% after 100 cycles, which indicates a fast structure transformation from layer to spinel [34]. However, the discharge capacity of $Li_{1.2}Mn_{0.8}O_2$ and $Li_{1.2}Ni_{0.1}Mn_{0.7}O_2$ shows a trend of gradual increase by reason of the gradual activation of Li_2MnO_3 upon cycling. It should be noted that, $Li_{1.2}Mn_{0.8}O_2$ presents a much slower growth rate that the discharge capacity increases from 22.08 $mAh{\cdot}g^{-1}$ to 39.13 $mAh{\cdot}g^{-1}$ after 100 cycles, which is

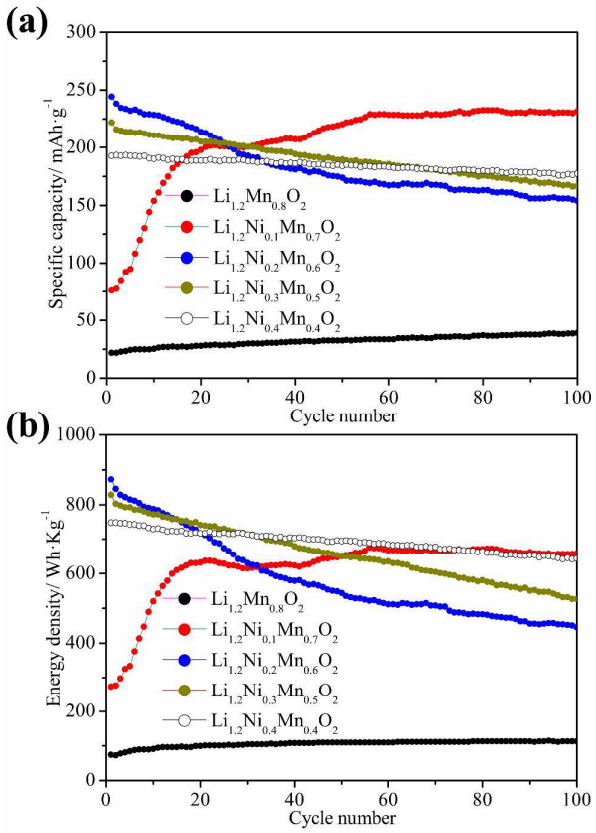

Fig. 5 (a) Cycling performances of all five samples at 0.1C between 2.0 V and 4.8 V. (b) Energy density curves of all the samples upon cycling at 0.1C.

attributed to the slow activation rate of Li_2MnO_3 suppressed by existing spinel phase $Li_{1+x}Mn_{2-x}O_4$ [31]. And for $Li_{1.2}Ni_{0.1}Mn_{0.7}O_2$, the discharge capacity reaches the highest value of 231.5 $mAh{\cdot}g^{-1}$ from the initial value of 76 $mAh{\cdot}g^{-1}$ after 75 cycles and still retains 100% of the capacity after 100 cycles. This phenomenon of capacity increase in the initial dozens of cycles is also ascribed to the gradual activation of Li_2MnO_3 caused by the existence of Mn^{3+}.

It is noted that $Li_{1.2}Ni_{0.3}Mn_{0.5}O_2$ and $Li_{1.2}Ni_{0.4}Mn_{0.4}O_2$ show excellent capacity retention with 75.04% and 92.13% after 100 cycles, respectively. The reason for this superior cyclic stability, which generally enhances as Ni^{3+} content increases, involves two aspects. One reason can be the reduction in Mn ion dissolution upon cycling resulting from decreasing the content of Mn, which leads to less capacity loss [16, 35]. The other reason is the reduction in Li ion irreversible dissolution and elimination of more Li vacancies upon cycling, for the smaller in size of Ni^{3+} than Ni^{2+} can't occupy the sites of Li layers after charge process, which can protect the active materials from structure transformation [16].

Voltage decay caused by the structure conversion from layer to spinel phase and the deterioration of the electrode/electrolyte interface is one of the main challenges for Li-rich cathode materials, which leads to the gradual decrease in energy density during cycling [36]. The charge-discharge curves of all five samples at various cycle numbers at 0.1C are employed to evaluate the voltage decay, as

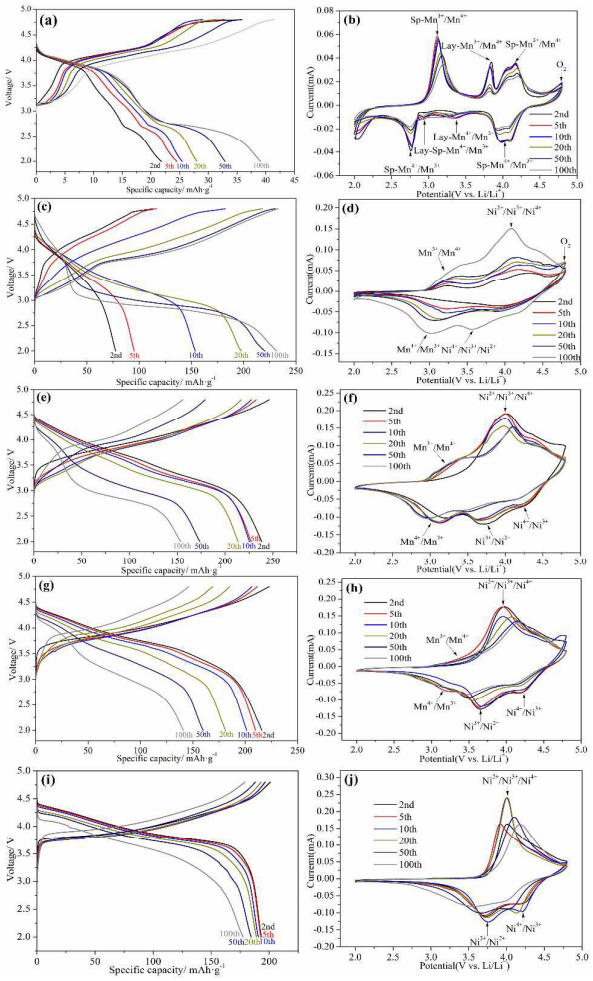

Fig. 6 Charge and discharge curves of (a) $Li_{1.2}Mn_{0.8}O_2$, (c) $Li_{1.2}Ni_{0.1}Mn_{0.7}O_2$, (e) $Li_{1.2}Ni_{0.2}Mn_{0.6}O_2$, (g) $Li_{1.2}Ni_{0.3}Mn_{0.5}O_2$ and (i) $Li_{1.2}Ni_{0.4}Mn_{0.4}O_2$ at 0.1C between 2.0 V and 4.8 V after the 2nd, 5th, 10th, 20th, 50th and 100th cycle. (b, d, f, h and j) Corresponding cyclic voltammetry profiles.

shown in Fig. 6, respectively. Severe voltage decay upon cycling is observed in $Li_{1.2}Mn_{0.8}O_2$ (Fig. 6a), $Li_{1.2}Ni_{0.1}Mn_{0.7}O_2$ (Fig. 6c) and $Li_{1.2}Ni_{0.2}Mn_{0.6}O_2$ (Fig. 6e), resulting from the unexpected layered-spinel structure transformation [37]. In particular, $Li_{1.2}Mn_{0.8}O_2$ exhibits an interesting gradual increase phenomenon of the discharge median voltage in the initial tens of cycles from 3.36 V to 3.60 V, for the proportion of $LiMnO_2$ with higher redox potential of Mn^{3+}/Mn^{4+} than $Li_{1+x}Mn_{2-x}O_4$ increases gradually along with the activation of Li_2MnO_3 [32]. However, the voltage fading rate efficiently slowed down with the increase of Ni^{3+} content, especially for $Li_{1.2}Ni_{0.4}Mn_{0.4}O_2$ with the voltage drop of 0.25 V. The alleviated voltage decay can be attributed to the enhancement of structural stability, the elimination of Li vacancies resulting from lower level of TM migration after charge process, the reduced Mn dissolution upon cycling and the weak interface reaction between electrode and electrolyte contributed by the reduction in oxygen release as the increase of Ni^{3+} [16, 37].

Fig. 6 (b, d, f, h and j) presents the CV curves of all materials after various cycles. It is obviously observed that the weak oxidation peaks of Li_2O removal from Li_2MnO_3 at 4.8 V always exist during 100 cycles for $Li_{1.2}Mn_{0.8}O_2$ (Fig. 6b), which proves the phenomenon of capacity increase upon cycling. Moreover, the oxidation peaks of Mn^{3+}/Mn^{4+} in spinel phase at about 3.2V continuously shift to a higher voltage upon cycling, and the reduction peaks of Mn^{4+}/Mn^{3+} in layer phase become weaker as well as a new reduction peak of 2.95 V occurs. This behavior can be interpreted that an unexpected layered-spinel intergrowth structure formation generates voltage decay and low capacity [11]. As shown in Fig. 6(d), a weak peak of oxygen release still appears in the 50th during charge process and disappears after 100 cycles, which verifies the interesting phenomenon of capacity change for $Li_{1.2}Ni_{0.1}Mn_{0.7}O_2$. In particular, the redox peak of Mn^{4+}/Mn^{3+} and the peak of Li_2MnO_3 activation cannot be observed all the time for $Li_{1.2}Ni_{0.4}Mn_{0.4}O_2$, indicating that traces of inactivated Li_2MnO_3 in active materials maybe enhance the structure and improve the voltage decay.

Fig. 5(b) shows the energy density profiles upon cycling, which are determined by capacity loss and voltage decay. $Li_{1.2}Ni_{0.2}Mn_{0.6}O_2$ delivers the highest initial energy density of 873 $Wh{\cdot}kg^{-1}$ and the lowest retention value of 446 $Wh{\cdot}kg^{-1}$ after 100 cycles. However, the gradual increase of capacity for $Li_{1.2}Ni_{0.1}Mn_{0.7}O_2$ and the excellent stability of capacity and voltage for $Li_{1.2}Ni_{0.4}Mn_{0.4}O_2$ exhibit much higher energy density of 660 $Wh{\cdot}kg^{-1}$ and 645 $Wh{\cdot}kg^{-1}$ after 100 cycles, respectively.

4. Conclusions

In this paper, a monoclinic-hexagonal layered material with a chemical formula of $Li_{1.2}Ni_xMn_{0.8-x}O_2$ (x=0, 0.1, 0.2, 0.3 and 0.4) was prepared by a combustion method to investigate the effect of valence states of Ni and Mn on the structure and electrochemical performances. A certain amount of Mn^{3+} in Li-rich cathode materials can be a useful approach to obtain the higher capacity and superior cyclability after the complete activation of Li_2MnO_3, while it will cause serious voltage decay. For example, $Li_{1.2}Ni_{0.1}Mn_{0.7}O_2$ reaches the highest discharge capacity of 231.5 $mAh{\cdot}g^{-1}$ from the initial value of 76 $mAh{\cdot}g^{-1}$ after 75 cycles and still keeps 100% of the capacity at 0.1C after 100 cycles, while the operating voltage drops from 3.60 V to 2.85 V after 100 cycles. In addition, Ni^{3+} plays an important role in improving the stability of capacity and voltage. And operating voltage increases with the content of Ni^{3+} because of the higher reduction potential of Ni^{4+}/Ni^{3+} compared with Ni^{4+}/Ni^{2+} and Mn^{4+}/Mn^{3+}. But Ni^{3+} will give rise to a lower discharge capacity for a little oxygen release. For instance, $Li_{1.2}Ni_{0.4}Mn_{0.4}O_2$ delivers the discharge capacity of 192.5 $mAh{\cdot}g^{-1}$ in the first cycle at 0.1C with the capacity retention of 92.13%, and initial operating voltage of 3.89 V with the voltage drop of 0.25 V after 100 cycles. Therefore, it is proposed that the amounts of Mn^{3+} and Ni^{3+} need to be well controlled during synthesis of Li-rich layered oxides to reach a reasonable integrated performance between high capacity, high operating voltage and excellent stability of capacity and voltage.

Acknowledgements

This work was supported by the China Postdoctoral Science Foundation (no. 2012M521760) and the Fundamental Research Funds for the Central Universities (no. xjj2014052).

References

1. M. S. Whittingham, *Chemical reviews*, 2004, **104**, 4271-4302.
2. G.-Y. Kim, S.-B. Yi, Y. J. Park and H.-G. Kim, *Materials Research Bulletin*, 2008, **43**, 3543-3552.
3. J. Yan, X. Liu and B. Li, *RSC Advances*, 2014, **4**, 63268-63284.
4. P. R. Ilango, T. Subburaj, K. Prasanna, Y. N. Jo and C. W. Lee, *Materials Chemistry and Physics*, 2015, **158**, 45-51.
5. J. Zheng, M. Gu, A. Genc, J. Xiao, P. Xu, X. Chen, Z. Zhu, W. Zhao, L. Pullan and C. Wang, *Nano letters*, 2014, **14**, 2628-2635.
6. M. M. Thackeray, C. S. Johnson, J. T. Vaughey, N. Li and S. A. Hackney, *Journal of Materials Chemistry*, 2005, **15**, 2257-2267.
7. J. Zheng, P. Xu, M. Gu, J. Xiao, N. D. Browning, P. Yan, C. Wang and J.-G. Zhang, *Chemistry of Materials*, 2015, **27**, 1381-1390.
8. M. Hou, J. Liu, S. Guo, J. Yang, C. Wang and Y. Xia, *Electrochemistry Communications*, 2014, **49**, 83-87.
9. Z. Lu and J. R. Dahn, *Journal of The Electrochemical Society*, 2002, **149**, A815-A822.
10. Y. Liu, Q. Wang, X. Wang, T. Wang, Y. Gao, M. Su and A. Dou, *Ionics*, 2015, **21**, 2725-2733.
11. T. Zhao, L. Li, R. Chen, H. Wu, X. Zhang, S. Chen, M. Xie, F. Wu, J. Lu and K. Amine, *Nano Energy*, 2015, **15**, 164-176.
12. D. Wang, Y. Huang, Z. Huo and L. Chen, *Electrochimica Acta*, 2013, **107**, 461-466.
13. D. Wang, I. Belharouak, G. Zhou and K. Amine, *Advanced Functional Materials*, 2013, **23**, 1070-1075.
14. L. Xiao, J. Xiao, X. Yu, P. Yan, J. Zheng, M. Engelhard, P. Bhattacharya, C. Wang, X.-Q. Yang and J.-G. Zhang, *Nano Energy*, 2015, **16**, 143-151.
15. X. Zhang, D. Luo, G. Li, J. Zheng, C. Yu, X. Guan, C. Fu, X. Huang and L. Li, *Journal of Materials Chemistry A*, 2013, **1**, 9721-9729.
16. J. C. Knight and A. Manthiram, *Journal of Materials Chemistry A*, 2015, **3**, 22199-22207.
17. L. Peng, Y. Zhu, U. Khakoo, D. Chen and G. Yu, *Nano Energy*, 2015, **17**, 36-42.
18. B. Li, C. Li, J. Cai and J. Zhao, *Journal of Materials Chemistry A*, 2015, **3**, 21290-21297.
19. M. E. Spahr, P. Novák, B. Schnyder, O. Haas and R. Nesper, *Journal of the electrochemical Society*, 1998, **145**, 1113-1121.
20. Z.-L. Gong, H.-S. Liu, X.-J. Guo, Z.-R. Zhang and Y. Yang, *Journal of power sources*, 2004, **136**, 139-144.
21. M. Xu, Z. Chen, H. Zhu, X. Yan, L. jun Li and Q. Zhao, *Journal of Materials Chemistry A*, 2015.
22. J. Lin, D. Mu, Y. Jin, B. Wu, Y. Ma and F. Wu, *Journal of Power Sources*, 2013, **230**, 76-80.
23. K. Shaju, G. S. Rao and B. Chowdari, *Electrochimica Acta*, 2002, **48**, 145-151.
24. H. Zhang, Q. Qiao, G. Li, S. Ye and X. Gao, *Journal of Materials Chemistry*, 2012, **22**, 13104-13109.
25. B. Hwang, Y. Tsai, D. Carlier and G. Ceder, *Chemistry of Materials*, 2003, **15**, 3676-3682.
26. K. A. Jarvis, Z. Deng, L. F. Allard, A. Manthiram and P. J. Ferreira, *Chemistry of materials*, 2011, **23**, 3614-3621.
27. S.-H. Kang, P. Kempgens, S. Greenbaum, A. Kropf, K. Amine and M. Thackeray, *Journal of Materials Chemistry*, 2007, **17**, 2069-2077.
28. L. Xu, P. Hou, Y. Zhang, H. Zhang, D. Song, X. Shi, X. Wang and L. Zhang, *Journal of Materials Chemistry A*, 2015, **3**, 21219-21226.
29. J.-S. Kim, C. S. Johnson, J. T. Vaughey, M. M. Thackeray, S. A. Hackney, W. Yoon and C. P. Grey, *Chemistry of Materials*, 2004, **16**, 1996-2006.
30. M. Thackeray, A. De Kock, M. Rossouw, D. Liles, R. Bittihn and D. Hoge, *Journal of The Electrochemical Society*, 1992, **139**, 363-366.
31. D. Ye, K. Ozawa, B. Wang, D. Hulicova-Jurcakova, J. Zou, C. Sun and L. Wang, *Nano Energy*, 2014, **6**, 92-102.
32. J. R. Croy, D. Kim, M. Balasubramanian, K. Gallagher, S.-H. Kang and M. M. Thackeray, *Journal of The Electrochemical Society*, 2012, **159**, A781-A790.
33. L. Wang, G. Liu, W. Wu, D. Chen and G. Liang, *Journal of Materials Chemistry A*, 2015, **3**, 19497-19506.
34. L. Li, B. Song, Y. Chang, H. Xia, J. Yang, K. Lee and L. Lu, *Journal of Power Sources*, 2015, **283**, 162-170.
35. S. Shi, J. Tu, Y. Zhang, Y. Zhang, C. Gu and X. Wang, *Electrochimica Acta*, 2013, **109**, 828-834.
36. X. Liu, Q. Su, C. Zhang, T. Huang and A. Yu, *Acs Sustainable Chemistry & Engineering*, 2015.
37. B. Li, C. Li, J. Cai and J. Zhao, *J.mater.chem.a*, 2015.